

Spontaneous Symmetry Breaking of Cavity Vacuum and Emergent Gyrotropic Effects in Embedded moiré Superlattices

Zuzhang Lin,^{1,2} Hsun-Chi Chan,^{1,2} Wenqi Yang,^{1,2} Yixin Sha,² Cong Xiao,³ Shuang Zhang,^{1,2} and Wang Yao^{1,2,*}

¹New Cornerstone Science Lab, Department of Physics, The University of Hong Kong, Hong Kong, China

²HK Institute of Quantum Science & Technology, University of Hong Kong, Hong Kong, China

³Institute of Applied Physics and Materials Engineering, University of Macau, Taipa, Macau, China

(Dated: February 12, 2025)

In an electronic system, spontaneous symmetry breaking can arise from many-body interaction between electrons, leading to degenerate ground states distinguishable by emergent effects otherwise prohibited by the symmetry. Here we show that ultrastrong coupling of a mesoscopic electronic system to the vacuum of a cavity resonator can lead to another paradigm of spontaneous breaking of spatial symmetries in both systems. As a pertinent example, we consider the orbital gyrotropic effects in a moiré superlattice embedded in a THz split ring cavity resonator. Our mean-field and exact diagonalization calculations consistently demonstrate a spontaneous parity symmetry breaking in both the electronic ground state and the cavity vacuum, leading to two degenerate hybrid ground states distinguished by their opposite orbital gyrotropic Hall and magnetic effects. These sizable responses in the cavity-embedded moiré superlattice are highly tunable by both the cavity field polarization and interlayer bias on the moiré superlattice, providing an advanced platform for manipulating gyrotropic effects.

Electronic systems respond to external electric and magnetic fields in ways that are restricted by their inherent symmetries [1, 2]. The responses can be controlled by breaking the symmetries through applying strain, introducing defects, creating materials interface, etc., which in general lead to a definite form of the response of interest. Coulomb interaction between electrons can also spontaneously break symmetries by establishing many-body correlations at low temperature, leading to a degenerate set of ground states each with its unique responses that are originally prohibited.

Cavity vacuum control has recently emerged as a new frontier in the manipulation of electronic properties, exploiting the vacuum quantum fluctuations which can dress electronic states with virtual cavity photons. Experiments observed significant influences of vacuum fluctuations on a broad range of phenomena, such as integer and fractional quantum Hall effects [3, 4], metal-to-insulator transition [5], magneto-transport [6], and chemical reaction [7]. The exchange of virtual photons in the cavity vacuum can also mediate a plethora of electron correlation phenomena [8], including superconductivity [9, 10], superfluidity [11], and charge-density-wave [12]. Theoretical studies have also shown that vacuum fluctuation is capable of transmitting broken symmetries of cavity confinements to the electronic system [13–15]. The intriguing prospect of spontaneous symmetry breaking in both the cavity field and electronic systems, which could enable otherwise prohibited responses, remains an unexplored area.

Moiré superlattices of 2D atomic crystals embedded in metallic split-ring terahertz (THz) electromagnetic resonator can provide diverse opportunities for the exploration of cavity vacuum control [16]. The deep sub-wavelength confinement in the micron scale ring gap leads to dramatic enhancement of the vacuum quantum fluctuations in the ultra-strong light-matter coupling regime [3, 6, 17–23]. The formation of superlattices through twisting controlled moiré patterns leads to versatile engaging material properties and meV-scale band-

width and bandgap, ideal for exploring the various aspects of vacuum control by THz cavities. The cavity mode is well discretized in energy while spanning all over superlattice sites in its micron scale volume, defining a mesoscopic system where many electrons are coupled to a common fundamental cavity mode. This mesoscopic nature underlies the nonlocal character of the virtual photon mediated electron-electron interaction, leading to intriguing possibilities such as remote control of topological matter [16].

In this work, we present a paradigmatic example of spontaneous symmetry breaking simultaneously in the vacuum of a split-ring cavity resonator and in the ground state of an embedded mesoscopic moiré superlattice. We consider orbital gyrotropic Hall effect (OGHE) from Berry curvature dipole and orbital gyrotropic magnetic effect (OGME) from orbital magnetic moment dipole, which require breaking both the C_3 rotational symmetry and parity symmetry of the moiré superlattice. Employing mean-field calculation and exact diagonalization (ED), we find the ground states of the hybrid system display spontaneous symmetry-breaking, with a two-fold degeneracy marked by distinct gyrotropic tensors and cavity field, related by parity transformation. Notably, the vacuum field-induced gyrotropic effects are highly tunable by the polarization of the cavity field and the interlayer bias applied to the moiré superlattice. We emphasize that the emergence of the gyrotropic effect here is a novel symmetry breaking phenomenon arising from strong vacuum fluctuation, which imprints the C_3 symmetry breaking of cavity confinement to the moiré and triggers the spontaneous parity symmetry breaking in both the cavity field and the moiré. The dual role of cavity vacuum fluctuation can be generally explored in other symmetry-breaking physics.

Vacuum field-induced gyrotropic effects. Gyrotropic effects generally describe the linear response of a time-reversal-odd axial vector with respect to a time-reversal-even polar vector in nonmagnetic crystals. The response coefficient α_{ab}^i (we denote $i = H$ for OGHE and M for OGME), the so called

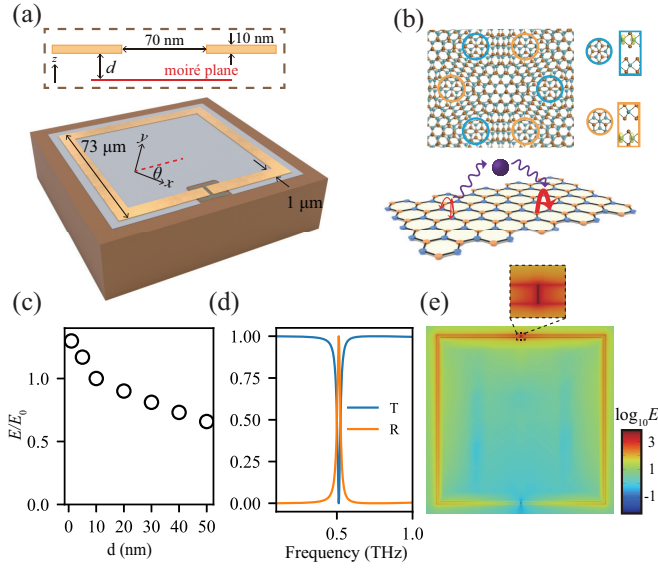


Figure 1. (a) Setup of the cavity-embedded moiré superlattice (the lower panel) encompassing a planar metallic split-ring Thz resonator (the gold ring) deposited on top of an h-BN substrate (the dark gray sheet). The upper panel shows a lateral perspective of the setup. (b) Illustration of the hexagonal moiré superlattice (the upper panel) composed of two moiré orbitals localized in the top (cyan circles) and bottom layers (orange circles), and the schematic diagram of the C_3 rotational symmetry breaking (the lower panel) as a result of distinct cavity vacuum field effects on holes' hopping across various directions. The thickness of the red arrows signifies the magnitude of the impact of the cavity vacuum field. (c) The electric field E averaged over a rectangular area of $0.3 \mu\text{m} \times 1 \mu\text{m}$, as a function of the vertical distance d . E_0 represents the value at $d = 10 \text{ nm}$. (d) Resonator's reflection and transmission spectra. (e) The cavity's electric field (in V/m) profile on the plane at a vertical distance $d = 20 \text{ nm}$ from the split-ring. The inset displays an enlarged view close to the gap.

gyrotropic tensors, can only be time-reversal even in nonmagnetic systems [24]. As such, the effects must involve carrier relaxation processes on the Fermi surface, and α_{ab}^i starts from the first order in relaxation time τ : $\alpha_{ab}^i = \tau R_{ab}^i$. Here R_{ab}^i is intrinsic to the band structures and reads [25–28]

$$R_{ab}^i = \int_{\text{BZ}} \frac{d^2k}{(2\pi)^2} v_a \frac{df}{d\varepsilon_k} B_{\mathbf{k},b}^i, \quad (1)$$

where $a, b = x, y, z$, \mathbf{v} is the band velocity, f is the Fermi-Dirac distribution function, and $\varepsilon_{\mathbf{k}}$ is the band energy. For OGHE (OGME), R^{H} (R^{M}) represents the Berry curvature dipole (orbital magnetic moment dipole), with B^{H} (B^{M}) symbolizing the momentum space Berry curvature (orbital magnetic moment). In two-dimension, $a = x, y$ (a represents the direction of the external field) and $b = z$ (z is set to perpendicular to the moiré plane) in Eq. (1) and R_{ab}^i can be abbreviated as R_a^i for brevity. Obviously, R_a^i is forbidden under parity and any rotational symmetry along z axis.

The moiré superlattice by itself preserves the C_{3z} rotational symmetry, thus prohibiting any tensor elements R_a^i . When placed in the proximity of the cavity gap, carrier hopping

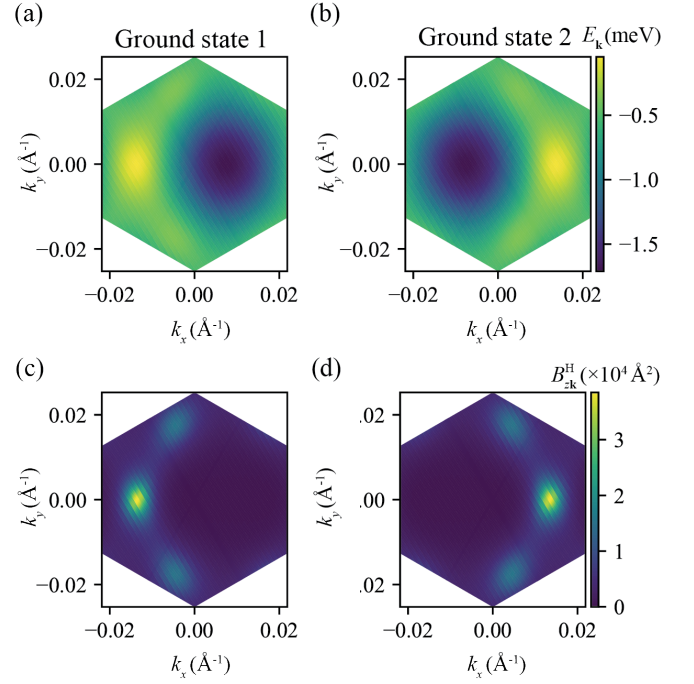


Figure 2. (a), (b) Mean-field dispersions for the lower miniband of the cavity renormalized moiré superlattice in its two degenerate ground states respectively. (c), (d) The corresponding band Berry curvature ($B_{z\mathbf{k}}^{\text{H}}$) in (a) and (b).

in the superlattice is influenced by the cavity vacuum field (Fig. 1), which breaks the C_{3z} symmetry. Nevertheless, both the moiré and the cavity mode here have the parity symmetry, which still forbids R_a^i . The gyrotropic effects can only emerge from spontaneous parity symmetry breaking, as the collective interplay of many carriers in the mesoscopic moiré superlattice and the virtual cavity photon, as demonstrated by the mean-field and exact diagonalization results in the following sections.

Model of the cavity-embedded moiré superlattice. We consider a single-gap resonator with a geometry schematically shown in Fig. 1(a). The resonant frequency for the fundamental cavity mode is 0.512 THz [Fig. 1(d)]. The mode has an electric field distribution highly concentrated in the vicinity of the gap region [c.f. Fig. 1(e)], where the moiré superlattice can be positioned to experience a strong vacuum field. The simulation of the THz resonator is performed via COMSOL Multiphysics software and the details can be found in the Section VI of the Supplemental Material.

The moiré superlattice under consideration is the homobilayer transition metal dichalcogenides with a small twist from the R-type stacking [Fig. 1 (b)]. Its lowest energy valence states at the \mathbf{K} (\mathbf{K}') valley can be effectively represented by a two-band tight-binding (TB) model on a honeycomb superlattice, with complex amplitude for the next-nearest-neighbor hopping originating from the real-space Berry curvature [29], which is essentially the Haldane model. We consider only one valley, as the other valley contributes equivalently to the

gyrotropic effects [30]. The Hamiltonian of the superlattice coupling to the cavity field reads,

$$H_m = \sum_{k\delta} \left(t_1 e^{i\mathbf{k}\cdot\delta} e^{i\chi\xi_\delta(a+a^\dagger)} c_{Bk}^\dagger c_{Ak} + \text{h.c.} \right) + \sum_{k\tau\mu} \left(t_2 e^{i\phi_\mu} e^{i\mathbf{k}\cdot\tau} e^{i\chi\xi_\tau(a+a^\dagger)} c_{\mu k}^\dagger c_{\mu k} + \text{h.c.} \right) \quad (2)$$

where $\mu = A, B$ denote the two sublattice sites, t_1 and t_2 respectively refer to the nearest- and next-nearest-neighbor hopping strength, ϕ_μ is the phase of the next-nearest-neighbor hopping, δ and τ are respectively the nearest- and next-nearest-neighbor hopping vectors. $\phi_\mu = 2\pi/3$ for $\mu = A$ and $-2\pi/3$ for $\mu = B$. The cavity field vector potential is $\mathbf{A} = A_0 \mathbf{e}_p (a + a^\dagger)$, with a^\dagger (a) the photon creation (annihilation) operator, and A_0 and \mathbf{e}_p the amplitude and directional unit vector of the cavity field, respectively. The coupling strength χ is defined as $eA_0|\delta|/\hbar$, and $\xi_\delta = \mathbf{e}_p \cdot \frac{\delta}{|\delta|}$, $\xi_\tau = \mathbf{e}_p \cdot \frac{\tau}{|\tau|}$. The Hamiltonian H_m is invariant under the parity transformation.

To capture the low-energy physics of the Hamiltonian in Eq. (2), we employ the Schrieffer-Wolff transformation [31] to project the total Hamiltonian $H_{\text{tot}} = H_m + H_c$ ($H_c = \hbar\omega a^\dagger a$ is the bare photon Hamiltonian) to the lowest-energy subspace (photon number $n = 0$). The effective Hamiltonian reads

$$H_0^{\text{eff}} = \langle 0|H_m|0\rangle + \sum_{l>0} U_l V_l, \quad (3)$$

where $U_l = \sum_{\mathbf{k}\mu\nu} P_{\mathbf{k}\mu} \langle 0|H_m|l\rangle P_{\mathbf{k}\nu} l\hbar\omega / [(E_{\mathbf{k}\mu} - E_{\mathbf{k}\nu})^2 - (l\hbar\omega)^2]$, $V_l = \sum_{\mathbf{k}\mu\nu} P_{\mathbf{k}\mu} \langle l|H_m|0\rangle P_{\mathbf{k}\nu}$ with $P_{\mathbf{k}\mu} = |\mathbf{k}\mu\rangle\langle\mathbf{k}\mu|$ the projection operator, l is the photon number index and $E_{\mathbf{k}\mu,l} = E_{\mathbf{k}\mu} + l\hbar\omega$. More details can be found in Sections II and III of the Supplemental Material.

Results from mean-field and exact diagonalization calculations. The term of product of four fermionic operators ($U_l V_l$) represents the interaction between holes via the exchange of virtual cavity photons. These terms can be treated using mean-field approximation, which leads to a mean-field Hamiltonian $H_{\text{mf}} \approx \langle 0|H_m|0\rangle + \sum_{l>0} (\langle U_l \rangle V_l + U_l \langle V_l \rangle - \langle U_l \rangle \langle V_l \rangle)$ that must be solved self-consistently (details can be found in Section III of the Supplemental Material). It is noted that the Hamiltonian of Eq. (3) is invariant under parity transformation, adhering to the system's parity symmetry. Yet, the mean-field Hamiltonian experiences a spontaneous parity symmetry breaking when the nonzero order parameters $\langle U_l \rangle$ and $\langle V_l \rangle$ are solved self-consistently.

Based on the established mean-field Hamiltonian, we next perform calculations to demonstrate the vacuum field-induced gyrotropic effects. We consider the moiré superlattice of a mesoscopic size in a rectangular region with dimensions of $0.3 \mu\text{m}$ by $1 \mu\text{m}$. Assuming the lattice plane has a vertical distance of $d = 20 \text{ nm}$ from that of the metal ring, the amplitude of the cavity electric field at the lattice can lead to a $\chi \approx 0.03$ (see more details in the Section VI of Supplemental Material). In the mean field calculations, the hopping amplitudes

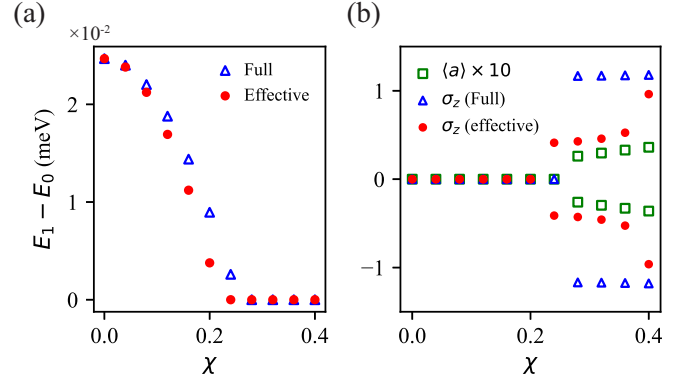


Figure 3. Exact diagonalization calculations. (a) Difference between the two lowest energy eigenvalues, and (b) orbital polarization (c.f. main text), with the increase of cavity coupling strength χ . Solid red circles are from ED calculations of the effective Hamiltonian of cavity-mediated hole-hole interaction (Eq. (3)). Hollow blue triangles are from ED of the full Hamiltonian of superlattice-cavity coupled system (Eq. (2)). ED of the full Hamiltonian also gives the expectation value of cavity field $\langle a \rangle$, shown by hollow green squares in (b).

are taken as $t_1 = 0.35 \text{ meV}$ and $t_2 = 0.1 \text{ meV}$, the derivative of Fermi Dirac distribution $\frac{df}{d\epsilon}$ is taken as a Gaussian function of width 0.15 meV , and we consider a filling factor of 0.9 hole per supercell.

Remarkably, the mean-field ground state features a two fold degeneracy. The energy dispersion of the mean-field bands differ a lot for the two ground states [Fig. 2(a) and (b)] and obviously break C_3 rotational symmetry. The distinct band dispersions for the two ground states are further accompanied by their different momentum-space Berry curvature ([Fig. 2(c) and (d)]) and orbital magnetic moment (Fig. S4 of the Supplemental Material). Notably, Berry curvature dipoles and orbital magnetic moment dipole are not only nonzero but opposite for these two ground states, which suggests that the parity symmetry is spontaneously broken in the ground states, and the two degenerate ground states are related by the parity transformation (more details in the Section IV of the Supplemental Material).

To further validate the proposition that a spontaneous parity symmetry breaking can indeed develop from the parity-symmetric cavity-mediated hole-hole interaction Eq. (3) or the full Hamiltonian of superlattice-cavity coupled system Eq. (2), we also perform exact diagonalization (ED) calculations with both Hamiltonians on a 3 by 5 unit-cell cluster on a torus geometry. The hole number is set to 14. Upon increasing the coupling strength χ , the difference between the two lowest energy eigenvalues gradually decreases [Fig. 3(a)] and vanishes for $\chi > 0.24$, indicating a two-fold degeneracy of the many-body ground state. The observed double degeneracy in ED calculations validates the one identified in mean-field calculations. Meanwhile, the orbital polarization $\sigma_z = \sum_{\mathbf{k}} (c_{A\mathbf{k}}^\dagger c_{A\mathbf{k}} - c_{B\mathbf{k}}^\dagger c_{B\mathbf{k}})$ becomes nonzero and in contrast for the two degenerate states [Fig. 3(b)]. Since

orbital polarization is prohibited by parity symmetry, it can serve as an indicator for parity symmetry breaking. ED calculations based on the cavity-mediated hole-hole interaction Hamiltonian Eq. (3) and that based on the full Hamiltonian of superlattice-cavity coupled system Eq. (2) agree well. ED of the full Hamiltonian also gives opposite expectation value $\langle a \rangle$ in the two degenerate ground states, showing the parity symmetry breaking in the cavity vacuum field. A more detailed discussion of ED calculations can be found in Section V in the supplementary material.

Upon determining the gyrotropic effects for a given set of parameters, we proceed to investigate the dependence of the R_a on the direction of the cavity field polarization and the onsite energy difference. Denote the cavity polarization as $e_p = (\cos \theta, \sin \theta)$ with $\theta = 0$ corresponding to the polarization pointing along the x direction. The gyrotropic tensor R_a exhibits a sinusoidal-like dependence on the variable θ [Figs. 4(a)-4(c)], resulting in both R_x and R_y encompassing positive and negative values. Throughout the range of the variable θ , an inverse relationship between R_a for two ground states is consistently observed. Intriguingly, it turns out that when the cavity field polarization is adjusted to along the y direction ($\theta = \pi/2 + N\pi$ with N as an integer), we find $R_x = 0$ but $R_y \neq 0$, whereas for cavity polarization along the x direction ($\theta = N\pi$), $R_y = 0$ but $R_x \neq 0$. The underlying mechanism is that the system upholds C_{2x} and C_{2y} for the former and latter case, and thus forbids R_x and R_y , respectively. Therefore, the occurrence of solely one gyrotropic tensor component (either R_x or R_y) for a particular cavity configuration is realized.

The emergent gyrotropic effects can be further controlled by a modest interlayer bias Δ , which introduces on-site energy difference between the two sublattices of the moiré polarized in opposite layers [c.f. Fig. 1(b)]. Figure 4(d) illustrates the interlayer bias dependence of the Berry curvature dipole. Clearly, when a finite Δ is introduced, R_y^H emerges due to the breaking of the C_{2y} symmetry, and the amplitude of R_x^H simultaneously changes. One notices that the ground state degeneracy is absent at finite interlayer bias, which explicitly break the parity symmetry. All gyrotropic tensor components in the ground state under a given interlayer bias is inversely related to those under the opposite interlayer bias. Moreover, Δ can induce a topological phase transition in the moiré superlattice. Remarkably, we find the topological transition is always accompanied by a continuous sign change of the R_x^H , as shown by the example in Fig. 4(d).

Discussion and conclusion. We note that in the literature exploring superradiant phase transition for the cavity vacuum, the possible occurrence of photon condensation marked by nonzero $\langle a \rangle$ has been extensively debated [32–37]. In contrast to such phase that is characterized by the presence of ground-state coherent photons in a macroscopic system, our focus inherently deviates towards an entirely different scenario, namely, a mesoscopic configuration where the thermodynamic limit is not applicable. Our ED calculation on a mesoscopic system unambiguously demonstrates the occurrence of nonzero $\langle a \rangle$, as a signature of the spontaneous parity

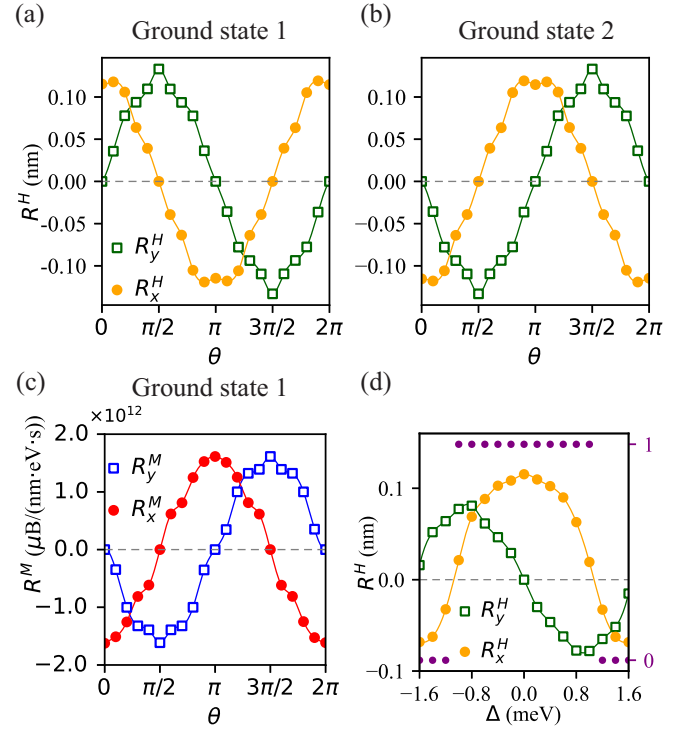


Figure 4. (a)-(b) Dependence of Berry curvature dipole on cavity field polarization for two degenerate ground states, when the interlayer bias applied to the moiré is set to zero. (c) The GME tensor Γ vs cavity field polarization for ground state 1, using the same calculations parameters of (a) and (b). (d) Dependence of Berry curvature dipole on interlayer bias when cavity field polarization is set to along the x axis ($\theta = 0$). The purple scatters refer to the Chern number. In all calculations, the filling factor f is maintained at 0.9, and scatter points are calculated, while the connecting lines merely enhance readability.

symmetry breaking in the cavity vacuum.

In conclusion, we have shown that strong light matter interaction in a moiré superlattice embedded in the vacuum of a split-ring THz resonator can lead to a spontaneous parity symmetry-breaking in the cavity vacuum and emergent gyrotropic effects of the embedded moiré superlattice. The vacuum field-induced gyrotropic effects possess significant magnitudes as compared to existing mechanisms in 2D materials [38–41], and can be effectively modulated by cavity field polarization and the interlayer bias, underlying a remarkable tunability as compared to those mechanisms relying on strain or introducing interface to break symmetry. Furthermore, spin-orbit coupling is absent in this vacuum field-induced gyrotropic effects, despite the prevailing notion that gyrotropic effects generally necessitate the spin orbit coupling.

Acknowledgment: The work is supported by Research Grant Council of Hong Kong SAR (A-HKU705/21, HKU SRFS2122-7S05, AoE/P-701/20), National Key R&D Program of China (2020YFA0309600), and New Cornerstone Science Foundation.

* wangyao@hku.hk

- [1] M. S. Dresselhaus, G. Dresselhaus, and A. Jorio, *Group theory: application to the physics of condensed matter* (Springer-Verlag, Berlin, 2008).
- [2] M. L. Cohen and S. G. Louie, *Fundamentals of condensed matter physics* (Cambridge University Press, 2016).
- [3] F. Appugliese, J. Enkner, G. L. Paravicini-Bagliani, M. Beck, C. Reichl, W. Wegscheider, G. Scalari, C. Ciuti, and J. Faist, Breakdown of topological protection by cavity vacuum fields in the integer quantum Hall effect, *Science* **375**, 1030 (2022).
- [4] J. Enkner, L. Graziotto, D. Boriçi, F. Appugliese, C. Reichl, G. Scalari, N. Regnault, W. Wegscheider, C. Ciuti, and J. Faist, Enhanced fractional quantum hall gaps in a two-dimensional electron gas coupled to a hovering split-ring resonator, arXiv preprint arXiv:2405.18362 (2024).
- [5] G. Jarc, S. Y. Mathenggattil, A. Montanaro, F. Giusti, E. M. Rigoni, R. Sergo, F. Fassioli, S. Winnerl, S. Dal Zilio, D. Mihailovic, P. Prelovšek, M. Eckstein, and D. Fausti, Cavity-mediated thermal control of metal-to-insulator transition in 1T-TaS₂, *Nature* **622**, 487 (2023), publisher: Nature Publishing Group.
- [6] G. L. Paravicini-Bagliani, F. Appugliese, E. Richter, F. Valmorra, J. Keller, M. Beck, N. Bartolo, C. Rössler, T. Ihn, K. Ensslin, C. Ciuti, G. Scalari, and J. Faist, Magneto-transport controlled by Landau polariton states, *Nat. Phys.* **15**, 186 (2019).
- [7] A. Thomas, L. Lethuillier-Karl, K. Nagarajan, R. M. A. Vergauwe, J. George, T. Chervy, A. Shalabney, E. Devaux, C. Genet, J. Moran, and T. W. Ebbesen, Tilting a ground-state reactivity landscape by vibrational strong coupling, *Science* **363**, 615 (2019), publisher: American Association for the Advancement of Science.
- [8] A. Frisk Kockum, A. Miranowicz, S. De Liberato, S. Savasta, and F. Nori, Ultrastrong coupling between light and matter, *Nat. Rev. Phys.* **1**, 19 (2019).
- [9] F. Schlawin, A. Cavalleri, and D. Jaksch, Cavity-mediated electron-photon superconductivity, *Phys. Rev. Lett.* **122**, 133602 (2019).
- [10] H. Gao, F. Schlawin, M. Buzzi, A. Cavalleri, and D. Jaksch, Photoinduced electron pairing in a driven cavity, *Phys. Rev. Lett.* **125**, 053602 (2020).
- [11] F. Schlawin and D. Jaksch, Cavity-mediated unconventional pairing in ultracold fermionic atoms, *Phys. Rev. Lett.* **123**, 133601 (2019).
- [12] J. Li and M. Eckstein, Manipulating intertwined orders in solids with quantum light, *Phys. Rev. Lett.* **125**, 217402 (2020).
- [13] D. Sedov, V. Shirobokov, I. Iorsh, and I. Tokatly, Cavity-induced chiral edge currents and spontaneous magnetization in two-dimensional electron systems, *Phys. Rev. B* **106**, 205114 (2022).
- [14] Y. Ke, Z. Song, and Q.-D. Jiang, Vacuum-induced symmetry breaking of chiral enantiomer formation in chemical reactions, *Physical Review Letters* **131**, 223601 (2023).
- [15] E. Viñas Boström, A. Sriram, M. Claassen, and A. Rubio, Controlling the magnetic state of the proximate quantum spin liquid α -rucl₃ with an optical cavity, *npj Comput. Mater.* **9**, 202 (2023).
- [16] Z. Lin, C. Xiao, D.-P. Nguyen, G. Arwas, C. Ciuti, and W. Yao, Remote gate control of topological transitions in moiré superlattices via cavity vacuum fields, *Proc. Natl. Acad. Sci. U. S. A.* **120**, e2306584120 (2023).
- [17] C. Ciuti, Cavity-mediated electron hopping in disordered quantum hall systems, *Phys. Rev. B* **104**, 155307 (2021).
- [18] G. Arwas and C. Ciuti, Quantum electron transport controlled by cavity vacuum fields, *Phys. Rev. B* **107**, 045425 (2023).
- [19] G. Scalari, C. Maissen, D. Turčinková, D. Hagenmüller, S. De Liberato, C. Ciuti, C. Reichl, D. Schuh, W. Wegscheider, M. Beck, and J. Faist, Ultrastrong Coupling of the Cyclotron Transition of a 2D Electron Gas to a THz Metamaterial, *Science* **335**, 1323 (2012).
- [20] H.-T. Chen, A. J. Taylor, and N. Yu, A review of metasurfaces: physics and applications, *Rep. Prog. Phys.* , 41 (2016).
- [21] J. Keller, G. Scalari, S. Cibella, C. Maissen, F. Appugliese, E. Giovine, R. Leoni, M. Beck, and J. Faist, Few-Electron Ultrastrong Light-Matter Coupling at 300 GHz with Nanogap Hybrid LC Microcavities, *Nano Lett.* **17**, 7410 (2017).
- [22] M. Jeannin, G. Mariotti Nesurini, S. Suffit, D. Gacemi, A. Vasanelli, L. Li, A. G. Davies, E. Linfield, C. Sirtori, and Y. Todorov, Ultrastrong light-matter coupling in deeply sub-wavelength thz lc resonators, *ACS photonics* **6**, 1207 (2019).
- [23] G. L. Paravicini-Bagliani, G. Scalari, F. Valmorra, J. Keller, C. Maissen, M. Beck, and J. Faist, Gate and magnetic field tunable ultrastrong coupling between a magnetoplasmon and the optical mode of an LC cavity, *Phys. Rev. B* **95**, 205304 (2017).
- [24] D. Culcer and R. Winkler, Generation of spin currents and spin densities in systems with reduced symmetry, *Phys. Rev. Lett.* **99**, 226601 (2007).
- [25] I. Sodemann and L. Fu, Quantum Nonlinear Hall Effect Induced by Berry Curvature Dipole in Time-Reversal Invariant Materials, *Phys. Rev. Lett.* **115**, 216806 (2015).
- [26] S. Zhong, J. E. Moore, and I. Souza, Gyrotropic Magnetic Effect and the Magnetic Moment on the Fermi Surface, *Phys. Rev. Lett.* **116**, 077201 (2016).
- [27] E. J. König, M. Dzero, A. Levchenko, and D. A. Pesin, Gyrotropic hall effect in berry-curved materials, *Phys. Rev. B* **99**, 155404 (2019).
- [28] Z. Z. Du, H.-Z. Lu, and X. Xie, Nonlinear hall effects, *Nat. Rev. Phys.* **3**, 744 (2021).
- [29] H. Yu, M. Chen, and W. Yao, Giant magnetic field from moiré induced berry phase in homobilayer semiconductors, *Natl. Sci. Rev.* **7**, 12 (2020).
- [30] Incorporating the other valley necessitates a TB model that encapsulates the physics of both valley, the primary effect of which is doubling the number of holes in comparison to the model detailed in the main text. The essence of the physics in this work can be addressed by integrating one valley.
- [31] J. R. Schrieffer and P. A. Wolff, Relation between the Anderson and Kondo Hamiltonians, *Phys. Rev.* **149**, 491 (1966).
- [32] K. Hepp and E. H. Lieb, On the superradiant phase transition for molecules in a quantized radiation field: the dicke maser model, *Ann. Phys.* **76**, 360 (1973).
- [33] Y. K. Wang and F. Hioe, Phase transition in the dicke model of superradiance, *Phys. Rev. A* **7**, 831 (1973).
- [34] P. Nataf and C. Ciuti, No-go theorem for superradiant quantum phase transitions in cavity QED and counter-example in circuit QED, *Nat Commun* **1**, 72 (2010).
- [35] K. Rzażewski, K. Wódkiewicz, and W. Żakowicz, Phase transitions, two-level atoms, and the a 2 term, *Phys. Rev. Lett.* **35**, 432 (1975).
- [36] O. Viehmann, J. von Delft, and F. Marquardt, Superradiant Phase Transitions and the Standard Description of Circuit QED, *Phys. Rev. Lett.* **107**, 113602 (2011), publisher: American Physical Society.
- [37] G. M. Andolina, F. M. D. Pellegrino, V. Giovannetti, A. H. MacDonald, and M. Polini, Cavity quantum electrodynamics

- of strongly correlated electron systems: A no-go theorem for photon condensation, *Phys. Rev. B* **100**, 121109 (2019).
- [38] Q. Ma, S.-Y. Xu, H. Shen, D. MacNeill, V. Fatemi, T.-R. Chang, A. M. Mier Valdivia, S. Wu, Z. Du, C.-H. Hsu, S. Fang, Q. D. Gibson, K. Watanabe, T. Taniguchi, R. J. Cava, E. Kaxiras, H.-Z. Lu, H. Lin, L. Fu, N. Gedik, and P. Jarillo-Herrero, Observation of the nonlinear Hall effect under time-reversal-symmetric conditions, *Nature* **565**, 337 (2019).
- [39] K. Kang, T. Li, E. Sohn, J. Shan, and K. F. Mak, Nonlinear anomalous Hall effect in few-layer WTe₂, *Nat. Mater.* **18**, 324 (2019), publisher: Nature Publishing Group.
- [40] J. Son, K.-H. Kim, Y. Ahn, H.-W. Lee, and J. Lee, Strain Engineering of the Berry Curvature Dipole and Valley Magnetization in Monolayer MoS_2 , *Phys. Rev. Lett.* **123**, 036806 (2019), publisher: American Physical Society.
- [41] E. Lesne, Y. G. Sağlam, R. Battilomo, M. T. Mercaldo, T. C. Van Thiel, U. Filippozzi, C. Noce, M. Cuoco, G. A. Steele, C. Ortix, and A. D. Caviglia, Designing spin and orbital sources of Berry curvature at oxide interfaces, *Nat. Mater.* **22**, 576 (2023).